See derivation of scaling in section 4, and comparison to Clausius-Clapeyron in Figure 6

# Scaling of Precipitation Extremes over a Wide Range of Climates Simulated with an Idealized GCM

PAUL A. O'GORMAN* AND TAPIO SCHNEIDER

*California Institute of Technology, Pasadena, California*

(Manuscript received 30 June 2008, in final form 8 April 2009)

ABSTRACT

Extremes of precipitation are examined in a wide range of climates simulated with an idealized aquaplanet GCM. The high percentiles of daily precipitation increase as the climate warms. Their fractional rate of increase with global-mean surface temperature is generally similar to or greater than that of mean precipitation, but it is less than that of atmospheric (column) water vapor content. A simple scaling is introduced for precipitation extremes that accounts for their behavior by including the effects of changes in the moist-adiabatic lapse rate, the circulation strength, and the temperature when the extreme events occur. The effects of changes in the moist-adiabatic lapse rate and circulation strength on precipitation extremes are important globally, whereas the difference in the mean temperature and the temperature at which precipitation extremes occur is important only at middle to high latitudes.

## 1. Introduction

The strong increase in the water vapor content of the atmosphere with increasing temperature means that climate warming is associated with major changes in the hydrological cycle. In simulations of global warming scenarios, atmospheric water vapor content increases with global-mean surface temperature at a rate of approximately 7.5% $K^{-1}$ (Held and Soden 2006). Horizontal moisture fluxes also strengthen, leading to an accentuation of the geographical pattern of evaporation minus precipitation (Held and Soden 2006; Lorenz and DeWeaver 2007). To the extent that floods and droughts result from anomalous horizontal moisture flux convergence or divergence, their intensity might be expected to increase as the climate warms (Held and Soden 2006). Analogously, Trenberth (1999) argued that a given storm will have higher precipitation rates in a warmer and moister climate because the precipitation over the storm lifetime is governed not by the local evaporation rate but by how much moisture converges at the base of the storm. It has been suggested that the heaviest precipitation events should increase proportionately to the atmospheric water vapor content, with even greater increases possible if the circulation strength increases (Allen and Ingram 2002; Trenberth et al. 2003; Pall et al. 2007). Such large increases in precipitation extremes would have important consequences for society and would be much greater than those expected for mean precipitation, which is energetically constrained (e.g., O'Gorman and Schneider 2008a).

There is some observational evidence that the frequency of heavy precipitation in extratropical regions has increased in the twentieth century (Groisman et al. 2005). Climate models predict that the frequency of intense precipitation increases with global warming over much of the globe (e.g., Sun et al. 2007; Kharin et al. 2007). Support from climate models is mixed, however, for the scaling of precipitation extremes with atmospheric water vapor content. This is termed Clausius–Clapeyron scaling, because the mean relative humidity remains roughly constant (Trenberth et al. 2003; Held and Soden 2006). [We will generally use Clausius–Clapeyron scaling to refer to scaling with (column) water vapor content; see section 4a for a discussion of the relation to near-surface specific humidity.] Pall et al. (2007) found that precipitation extremes increased faster than mean precipitation in the Hadley Centre climate model, but with deviations from Clausius–Clapeyron scaling in the tropics and high latitudes. Kharin et al. (2007) examined

* Current affiliation: Massachusetts Institute of Technology, Cambridge, Massachusetts.

*Corresponding author address:* Paul O'Gorman, Massachusetts Institute of Technology, Cambridge, MA 02139.
E-mail: pog@mit.edu

DOI: 10.1175/2009JCLI2701.1

precipitation extremes in coupled climate model simulations of global warming; they found a multimodel mean rate of increase with a global-mean surface temperature of 6% $K^{-1}$ for the globally averaged 20-yr return period precipitation. This is broadly consistent with Clausius–Clapeyron scaling, but confidence in this result is low because of considerable intermodel scatter.

There are several reasons why precipitation extremes may not scale with atmospheric water vapor content. For example, the strength of circulations does not need to stay constant as climate changes. Indeed, the strength of tropical circulations and convective mass fluxes are expected to decrease as the climate warms (Betts 1998; Held and Soden 2006). Arguments for the scaling of precipitation extremes have been made based on scenarios in which the atmosphere is dried out during an extreme event (Allen and Ingram 2002; Pall et al. 2007), or by considering the moisture convergence into a storm (Trenberth et al. 2003). However, it is unclear to what extent such simple arguments can be applied to the complex dynamics and thermodynamics of precipitating systems. In addition, the dependence of precipitation extremes on climate is complicated by the possibility that the mean temperature at a given location is not representative of the temperature when a precipitation extreme occurs.

One may also question whether current climate models can reliably simulate statistics of rare precipitation events, particularly in the tropics where moist convective parameterizations, which were not necessarily designed to capture high-order statistics of rainfall, are of central importance. Wilcox and Donner (2007) found that changes in the frequency of precipitation events exceeding a certain threshold were greater between two simulations using different convection schemes than for a 2-K surface warming using either convection scheme. Given this possible sensitivity to subgrid parameterizations, and given the difficulty in using past observations to assess the effect of climate change on precipitation extremes, it is essential to improve our physical understanding of the behavior of precipitation extremes.

Here we study how climate change influences precipitation extremes in an idealized general circulation model (GCM) of the atmosphere. We give physical arguments for how precipitation extremes depend on climate characteristics and why they should not be expected to scale with atmospheric water vapor content. Rather than studying changes in the frequency with which a fixed threshold of precipitation is exceeded, we instead analyze changes in the high percentiles of the daily precipitation distribution. This approach allows a direct comparison of fractional increases in extreme precipitation with fractional increases in water vapor content or mean precipitation (Allen and Ingram 2002; Pall et al. 2007).

The idealized GCM (section 2) employs simplified moist parameterizations (Frierson 2007), which are based on similar physical principles to those used in comprehensive climate models, but have fewer tunable parameters or thresholds that can influence the dependence of precipitation extremes on climate characteristics. The idealized GCM allows the simulation of a wide range of climates so that differences in the dependence of water vapor content, mean precipitation, and precipitation extremes on, for example, global-mean surface temperature can be easily discerned (section 3). We show that the fractional rate of increase in precipitation extremes with global-mean surface temperature is smaller than that of atmospheric water vapor content, and we account for this by using a scaling for precipitation extremes that allows for thermodynamical and dynamical changes (section 4).

## 2. Model and simulations

The idealized GCM and series of simulations are described in detail in O'Gorman and Schneider (2008a). The GCM is based on the hydrostatic primitive equations, discretized with 30 vertical sigma levels and a horizontal spectral resolution of T42. A subset of the simulations, discussed in section 3, was rerun at the higher horizontal resolution of T85. The GCM is configured as an ''aquaplanet'' for which the lower boundary is a uniform mixed-layer ocean of 0.5-m depth, with no horizontal heat transport and constant albedo. [A mixed layer depth of 1 m was incorrectly stated in O'Gorman and Schneider (2008a).] Insolation is imposed as a perpetual equinox with no diurnal cycle. Statistics of the simulated climates are thus steady and zonally and hemispherically symmetric.

Only the vapor liquid phase change of water is considered, and the latent heat of condensation is taken to be constant. A variant of the quasi-equilibrium scheme of Frierson (2007) parameterizes moist convection. When active, it relaxes temperatures toward a profile with a moist-adiabatic lapse rate and specific humidities toward a profile with a relative humidity of 70%. A 2-h relaxation time is used for both temperature and moisture. A grid-scale condensation scheme prevents gridbox supersaturation by adjusting the moisture field and accounting for latent heat release by adjusting the temperature field. There is no reevaporation of falling condensate.

Changes in climate are forced by changes in the optical thickness of an idealized longwave absorber, which represents the cumulative effects of all greenhouse gases. Because the longwave optical thickness is imposed, radiative water vapor feedback and radiative effects of clouds are not taken into account in the GCM.

Longwave radiation is treated using a two-stream gray radiation scheme with optical thickness specified as $\tau = \alpha\tau_{\text{ref}}$, where the reference distribution $\tau_{\text{ref}}$ is a fixed function of pressure and latitude. The longwave optical thickness is varied by setting the rescaling factor $\alpha$ to a different value in each of a series of 16 simulations. Each simulation is spun up to statistical equilibrium and then run for 600 more days. The reference simulation ($\alpha = 1$) has a global-mean surface temperature similar to that of present-day Earth.

The effect of climate change on the mean hydrological cycle, extratropical transient eddies, and extratropical thermal stratification in this series of simulations is investigated in O'Gorman and Schneider (2008a,b) and Schneider and O'Gorman (2008), respectively. Sampling variability causes slight differences between some mean quantities reported in this paper and in earlier papers because we have run the simulations for a longer time here to obtain statistics of precipitation extremes.

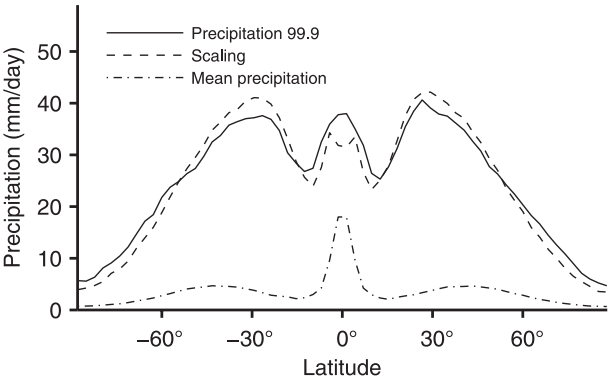


FIG. 1. The 99.9th percentile of daily precipitation (solid) and mean precipitation (dash–dotted) in the reference simulation ($\alpha = 1$). The precipitation extremes scaling (4) is also shown (dashed), multiplied by a constant of proportionality of 3.5 so that it agrees with the 99.9th percentile in the global mean. Statistics shown here and in the following figures are based on zonal and time averages. Deviations from symmetry between the hemispheres are indicative of sampling error.

## 3. Precipitation extremes in the idealized GCM

Because the model is statistically zonally symmetric, the precipitation extremes are analyzed on a latitude-by-latitude basis. The percentiles are estimated by aggregating the daily gridbox precipitation amounts (including days with zero precipitation) over time and longitude, and then linearly interpolating the cumulative distribution function of the sample. For example, the 99th percentile at a given latitude is the amount of daily precipitation exceeded with 1% probability in a given grid box at that latitude.

Figure 1 shows the meridional distribution of mean precipitation and of the 99.9th percentile of daily precipitation for the reference simulation ($\alpha = 1$). There are characteristic local maxima of both mean and extreme precipitation in the extratropics and deep tropics. The extratropical maxima of mean precipitation are farther poleward than the maxima of extreme precipitation.

The changes in mean and 99.9th percentile precipitation, as well as in column water vapor, are shown in Fig. 2 for a global-mean surface temperature increase of 6.1 K from the $\alpha = 1$ to the $\alpha = 1.4$ simulation. The global-mean surface temperature refers to the global-mean surface air temperature, which is the global-mean temperature at the lowest model level. Lower-tropospheric temperatures increase more strongly at high latitudes than in the tropics; this largely accounts for the greater increases in precipitation and water vapor content at high latitudes [see O'Gorman and Schneider (2008b) for an account of changes in the thermal structure of the atmosphere in these simulations]. The mean precipitation increases in the tropics and extratropics but decreases in the subtropics, whereas the 99.9th percentile precipitation increases at all latitudes. The increases in column water vapor exceed the increases in mean and extreme precipitation, except at the highest latitudes. The fractional rates of change with global-mean surface temperature of the column water vapor shown in Fig. 2, and of the tropospheric column integral of saturation specific humidity, differ by 0.65% $K^{-1}$ in the global mean, and by less than 1.8% $K^{-1}$ at each latitude, consistent with an approximately constant relative humidity in the lower troposphere, which dominates the column integrals.[1] Thus, Clausius–Clapeyron scaling and scaling with atmospheric water vapor content are roughly equivalent for these simulations.

The difference in behavior of extreme precipitation and atmospheric water vapor content is clearly evident when a wide range of climates is considered. Figure 3 shows the global-mean precipitation and water vapor content compared with the global mean of the 99.9th percentile precipitation at each latitude. The water vapor content grows almost exponentially (giving a straight line on the log-linear plot), which is again consistent with an approximately constant relative humidity in the lower

[1] In taking the vertical integral of saturation specific humidity, we exclude levels above the global-mean tropopause level. This is especially appropriate in the colder simulations, which have significant mass in the stratosphere. The tropopause is determined as the level with a mean temperature lapse rate of 2 K $km^{-1}$. The tropopause is poorly defined at high latitudes in the coldest simulation, and these latitudes are excluded from the meridional average that is used to determine the global-mean tropopause level for this simulation; see O'Gorman and Schneider (2008b).

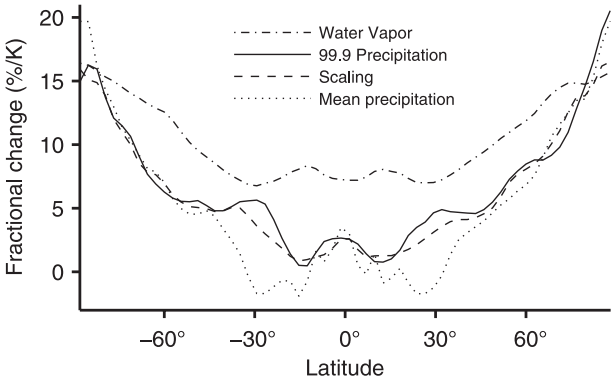


FIG. 2. Fractional changes between the reference simulation ($\alpha = 1$) and a warmer simulation ($\alpha = 1.4$) expressed as a percentage of the reference simulation values: column water vapor (dash–dotted), 99.9th percentile of daily precipitation (solid), precipitation extremes scaling (4) (dashed), and mean precipitation (dotted). The changes are normalized by the global-mean surface temperature difference of 6.1 K between the two simulations. The changes shown for the 99.9th percentile precipitation and the scaling have been smoothed in latitude with a 1–2–1 filter.

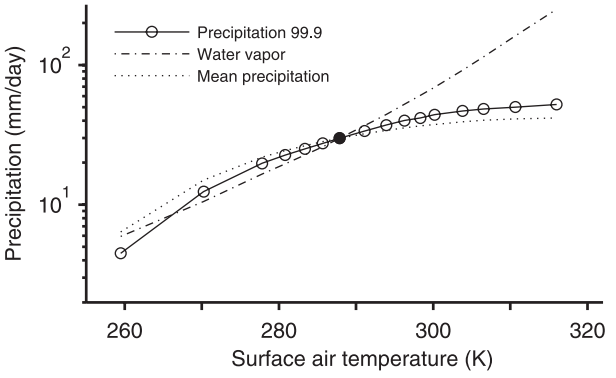


FIG. 3. Global mean of the 99.9th percentile precipitation rate vs global-mean surface temperature (solid line with circles) shown on a log-linear plot. The reference simulation is shown with a filled circle. Also shown is the rescaled global-mean water vapor content (dash–dotted) and the rescaled global-mean precipitation (dotted). Both the water vapor content and mean precipitation curves have been rescaled by dimensional constants so that they can be compared with the extreme precipitation and coincide with it at the reference simulation. At the reference simulation, the fractional rate of increase with global-mean surface temperature is 6.4% $K^{-1}$ for water vapor content, 3.8% $K^{-1}$ for the 99.9th percentile of precipitation, and 2.5% $K^{-1}$ for mean precipitation.

troposphere (O'Gorman and Schneider 2008a). The mean and extreme precipitation grow at a greater fractional rate than the water vapor content in the coldest climates, but at a much smaller fractional rate in moderate to warm climates.

Figure 4 shows the global-mean behavior of daily precipitation for several different high percentiles. As can be seen from the figure, although the absolute rates of increase vary systematically with temperature, a fractional rate of increase of 3% $K^{-1}$ relative to the reference climate is a rough approximation of the behavior of the precipitation extremes over a range of climates and percentiles. The fractional rates of increase at the reference simulation are shown in Fig. 5. The rate of change of the precipitation extremes with temperature increases for higher percentiles, but it remains lower than the rate of change of atmospheric water vapor content.

To test the resolution dependence of our results, a subset of the simulations was repeated at a higher spatial resolution of T85.[2] The numerical values of the precipitation extremes are higher in the higher-resolution runs. For example, in the reference simulation, the global mean of the 99.9th percentile increases from 29.9 mm $day^{-1}$ at T42 to 35.7 mm $day^{-1}$ at T85. Chen and Knutson (2008) argue that larger values of precipitation extremes should be expected in gridded data at higher spatial resolution if precipitation amounts are considered as areal averages over each grid box. The rate of increase in the global mean of the 99.9th percentile precipitation with global-mean surface temperature is 3.7% $K^{-1}$ at the reference simulation in the T85 simulations, which is slightly lower than the rate of increase in the T42 simulations (3.8% $K^{-1}$). The corresponding rate of increase in global-mean water vapor content also decreases in the higher-resolution run (from 6.4% to 6.2% $K^{-1}$).

We also tested the effect of using instantaneous rather than daily accumulated precipitation in our analysis of two simulations ($\alpha = 1, 1.4$). The fractional changes in precipitation extremes were similar for both daily and instantaneous precipitation. It is possible, however, that our GCM with parameterized convection does not properly capture the behavior of precipitation on short time scales (cf. Lenderink and van Meijgaard 2008).

## 4. Scaling of precipitation extremes

### a. *Derivation of scaling*

The scaling of precipitation extremes is approached in terms of the scaling of the condensation term in the evolution equation for specific humidity. We assume that condensation occurs at approximately fixed relative humidity (e.g., at saturation) and that the condensation is related to upward motion and adiabatic cooling. The instantaneous condensation rate $c$ (when nonzero) is then given by

$$c \sim -\omega \left. \frac{dq_s}{dp} \right|_{\theta^*}, \tag{1}$$

[2] Because of computational expense, the higher-resolution simulations were run for 300 days after spinup rather than 600 days.

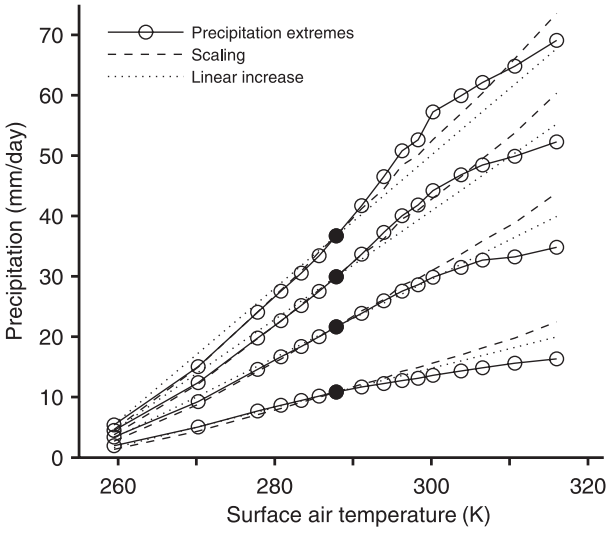


FIG. 4. Global mean of high percentiles of precipitation rate vs global-mean surface temperature (solid lines with circles). The reference simulation is shown with filled circles. The 90th, 99th, 99.9th, and 99.99th percentiles are shown in increasing order of precipitation rate. The precipitation extremes scaling (4) is shown with a dashed line for each percentile and has been normalized in each case to pass through the reference simulation value (with rescaling constants of 1.3, 2.6, 3.5, and 4.2). The dotted lines show linear increases at 3% $K^{-1}$ relative to the reference simulation.

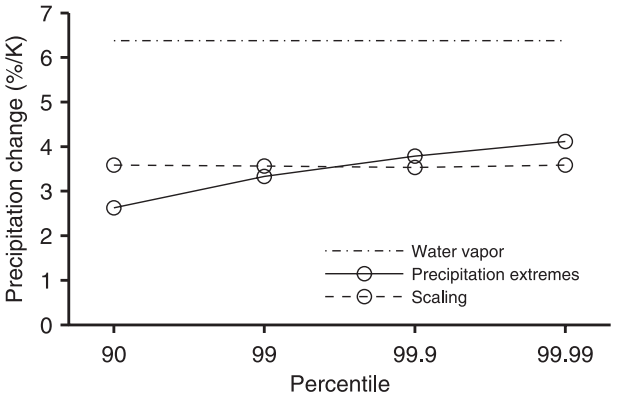


FIG. 5. Fractional rates of increase with global-mean surface temperature at the reference simulation for the global-mean precipitation extremes (solid), precipitation extremes scaling (4) (dashed), and water vapor content (dash–dotted). Values are shown for the 90th, 99th, 99.9th, and 99.99th percentiles. The rates of increase in the precipitation extremes are 2.6%, 3.3%, 3.8%, and 4.1% $K^{-1}$. The rates of increase in the scaling are 3.6%, 3.6%, 3.5%, and 3.6% $K^{-1}$. The rate of increase in the water vapor content is 6.4% $K^{-1}$.

where $\omega$ is the vertical velocity in pressure coordinates, $q_s$ is the saturation specific humidity, and $p$ is the pressure.[3] The derivative of saturation specific humidity with respect to pressure $dq_s/dp|_{\theta^*}$ must be taken at constant (saturation) equivalent potential temperature $\theta^*$ to allow for the warming effect of latent heat release. We will refer to $dq_s/dp|_{\theta^*}$ as the moist-adiabatic derivative of saturation specific humidity. It is a thermodynamic function of temperature and pressure and may be written in terms of the moist-adiabatic temperature lapse rate $dT/dp|_{\theta^*}$ as

$$\left.\frac{dq_s}{dp}\right|_{\theta^*} = \frac{\partial q_s}{\partial p} + \frac{\partial q_s}{\partial T}\left.\frac{dT}{dp}\right|_{\theta^*}. \qquad (2)$$

We assume that the limit of pseudoadiabatic ascent is adequate for the scaling of precipitation extremes.

The condensation scaling (1) implies that changes in the statistics of the vertical velocity $\omega$ will affect the magnitude of the condensation rate. The condensation scaling (1) will also differ from Clausius–Clapeyron scaling because the moist-adiabatic derivative of saturation specific humidity $dq_s/dp|_{\theta^*}$ does not generally scale with the saturation specific humidity, as shown in Fig. 6 (Betts and Harshvardhan 1987). This is primarily because the moist-adiabatic lapse rate $dT/dp|_{\theta^*}$ in Eq. (2) varies with temperature. In physical terms, the greater latent heat release at higher temperatures moderates the increase in the condensation rate needed to maintain constant relative humidity of an air parcel for a given upward velocity. The saturation specific humidity generally increases at a greater fractional rate with temperature than $dq_s/dp|_{\theta^*}$, with a greater difference in growth rates at higher temperatures. As a consequence, $dq_s/dp|_{\theta^*}$ will obey Clausius–Clapeyron scaling most closely at high latitudes, high in the troposphere, or in very cold climates, but it can behave quite differently in general. The form of the temperature dependence of $dq_s/dp|_{\theta^*}$ shown in Fig. 6 contributes to the greater fractional growth rate of precipitation extremes in colder climates (cf. Fig. 3). That the condensation rate does not obey Clausius–Clapeyron scaling means that we should not expect precipitation to obey it either (both for mean or extreme precipitation).

The condensation rate scaling (1) can also be related to the static stability along a moist adiabat (Iribarne and Godson 1981; Betts and Harshvardhan 1987). Along a moist adiabat, we have $dq_s \approx -(c_p/L)(T/\theta)\, d\theta$, where $\theta$ is the potential temperature, $L$ is the latent heat of condensation (assumed constant), and $c_p$ is the specific heat capacity of air. The condensation rate scaling (1) can then be written as

[3] If condensation maintains saturation of a rising air parcel so that the specific humidity approximately equals $q_s$, and if moisture sources other than condensation are neglected so that $c = -Dq_s/Dt$, and if diabatic effects other than latent heating are neglected so that the saturation equivalent potential temperature $\theta^*$ is conserved, then writing $q_s = q_s(p, \theta^*)$, we find $c = -dq_s/dp|_{\theta^*}\, Dp/Dt$. Equation (1) then follows from the definition of the vertical pressure velocity $\omega$.

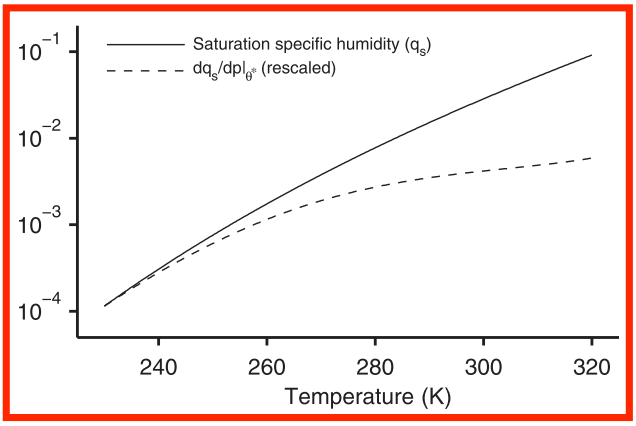


FIG. 6. Saturation specific humidity (solid) and the rescaled moist-adiabatic derivative of saturation specific humidity $dq_s/dp|_{\theta^*}$ (dashed). Both quantities are evaluated at a pressure of 800 hPa. The moist-adiabatic derivative of saturation specific humidity has been rescaled by a dimensional constant so that it agrees with the saturation specific humidity at the lowest temperature shown. At 280 K, the fractional rate of increase in saturation specific humidity is 6.9% $K^{-1}$, compared with 3.0% $K^{-1}$ for the moist-adiabatic derivative of saturation specific humidity.

$$c \sim \omega \frac{c_p T}{L\theta} \frac{d\theta}{dp}\bigg|_{\theta^*}. \tag{3}$$

This expression clearly shows the thermodynamic balance between the condensation rate (and its associated latent heating $Lc$) and the adiabatic cooling associated with upward motion. The static stability $d\theta/dp|_{\theta^*}$ increases with increasing temperature, but it does so at a smaller fractional growth rate than saturation water vapor, which is an alternative view of why the condensation rate increases less rapidly with temperature than Clausius–Clapeyron scaling would suggest.

A scaling for precipitation extremes can be obtained from Eq. (1) by assuming that the surface precipitation rate is proportional to the vertically integrated condensation rate, and by scaling the extreme upward velocity with the root-mean-square eddy vertical velocity $\omega_{\rm rms}$. The use of $\omega_{\rm rms}$ will not capture non-Gaussian changes in high-order statistics of the vertical velocity, but it should be adequate to capture some changes that accompany climate change, such as a meridional shift of the storm tracks (Yin 2005) or a decrease in tropical convective mass fluxes (Betts 1998; Held and Soden 2006). The resulting precipitation extremes scaling is

$$P_e \sim \int_{p_t}^{p_s} \frac{dp}{g} \omega_{\rm rms} \frac{dq_s}{dp}\bigg|_{\theta^*, T_e}, \tag{4}$$

where $P_e$ is a high percentile of precipitation (say the 99.9th percentile), the pressure integral is from the tropopause pressure $p_t$ to the surface pressure $p_s$, and $g$ is the acceleration due to gravity. The moist-adiabatic derivative of saturation specific humidity at each latitude and level is not evaluated at the local mean temperature, but at $T_e$, the local mean temperature conditioned on precipitation (at the surface) equaling the precipitation percentile. This allows for the possibility that the temperature at which precipitation extremes occur does not scale with the climatological mean temperature. Note that the temperature $T_e$ at a given level and latitude and for a given percentile of precipitation will generally not be equal to the corresponding percentile of the temperature distribution.

In the tropics, if the variation of $\omega_{\rm rms}$ is neglected, then the scaling (4) approximately obeys Clausius–Clapeyron scaling with respect to surface temperature. This is because the mean thermal stratification is approximately moist adiabatic in the tropics, and so the moist-adiabatic derivative of saturation specific humidity can be integrated with respect to pressure to give the surface saturation specific humidity (if the saturation specific humidity at the tropopause and the vertical variation of $\omega_{\rm rms}$ are neglected). The surface saturation specific humidity does not scale with column water vapor because of different temperature changes at different levels, which imply different specific humidity changes at different levels if the relative humidity is approximately invariant. Clausius–Clapeyron scaling with respect to surface temperature is a useful conceptual simplification for the scaling of tropical precipitation extremes, but changes in vertical velocity statistics in the tropics generally cannot be neglected, and there is no general basis for such a simplification in the extratropics.

In summary, the precipitation extremes scaling (4) need not obey Clausius–Clapeyron scaling (using mean temperature changes and column saturation water vapor content) because of changes in the moist-adiabatic lapse rate and possible changes in vertical velocity statistics, and if the temperature $T_e$ does not scale with the mean temperature.

### b. *Application to GCM simulations*

We apply the precipitation extremes scaling (4) at each latitude to the zonally and temporally averaged statistics of the idealized GCM. The GCM uses a sigma ($\sigma$) coordinate system, and so a sigma-coordinate formulation of the scaling is evaluated.[4] We use the simplified moist

[4] The rms eddy pressure velocity $\omega_{\rm rms}$ is replaced with the rms eddy sigma velocity $\dot{\sigma}_{\rm rms}$ multiplied by a reference surface pressure $p_0 = 10^5$ Pa. The pressure integral is replaced by $p_0$ multiplied by an integral in sigma from the surface to the global-mean level of the tropopause (see footnote 1). Use of the local tropopause level at each latitude gives similar results. The moist-adiabatic derivative of saturation specific humidity is evaluated on sigma levels at the precipitation extremes temperature $T_e$ but at the zonal and time mean pressure. Eddy quantities such as $\dot{\sigma}_{\rm rms}$ are derived from 4-times-daily instantaneous model output; precipitation and $T_e$ are based on daily averaged values.

thermodynamics of the idealized GCM in all calculations (e.g., we neglect the effect of water vapor on the heat capacity per unit mass of air and take the latent heat of condensation to be constant).

The temperature $T_e$ corresponding to precipitation extremes is evaluated at each latitude and sigma level using an average conditioned on the percentiles of daily surface precipitation in the simulations. To reduce noise, the average used in calculating $T_e$ for a given percentile is taken over all days and longitudes where the precipitation lies in a certain range, rather than exactly at the precipitation percentile. The range for the $n$th percentile is chosen at each latitude to be between the $100 - (3/2)(100 - n)$ and $100 - (1/2)(100 - n)$ percentiles of precipitation at that latitude. For example, in the case of the 99th percentile, we take a temperature average over all days and longitudes at which precipitation lies between the 98.5th and 99.5th percentiles.

Figure 7a shows the difference $T_e - \overline{T}$ in the reference simulation between the temperature corresponding to the 99.9th percentile of precipitation and the mean temperature. The temperature difference is largest in the extratropical troposphere and maximizes just poleward of the extratropical storm tracks, which are centered at roughly $\pm 50°$ latitude. The air is generally warmer when precipitation extremes occur, consistent with precipitation extremes at high latitudes occurring in warm and moist air masses that have moved poleward. The temperature difference is largest in the middle to high latitudes over the full range of simulations. The use of $T_e$ rather than the mean temperature in the precipitation extremes scaling (4) is important at these latitudes.

The precipitation extremes scaling (4) is shown for the reference simulation in Fig. 1. The scaling captures much of the meridional variation of the 99.9th percentile precipitation. This is somewhat surprising given the transition in precipitation from a mixture of resolved grid-scale condensation and subgrid convection in the extratropics to the almost entirely subgrid convection in the tropics (O'Gorman and Schneider 2008a). Whether this will hold true in other models or observations will likely depend on how representative the vertical velocity statistic $\omega_{\text{rms}}$ is of motions at different length scales.

In general, we would expect the scaling to more robustly predict changes in precipitation extremes with climate change than the meridional distribution of precipitation extremes in a given simulation. Figure 2 shows that the changes in the 99.9th percentile precipitation are well captured by the scaling at all latitudes for a global-mean increase in surface temperature of 6.1 K. Figure 4 shows reasonably good agreement between the scaling and changes in the global-mean extreme precipitation over the full range of climates.

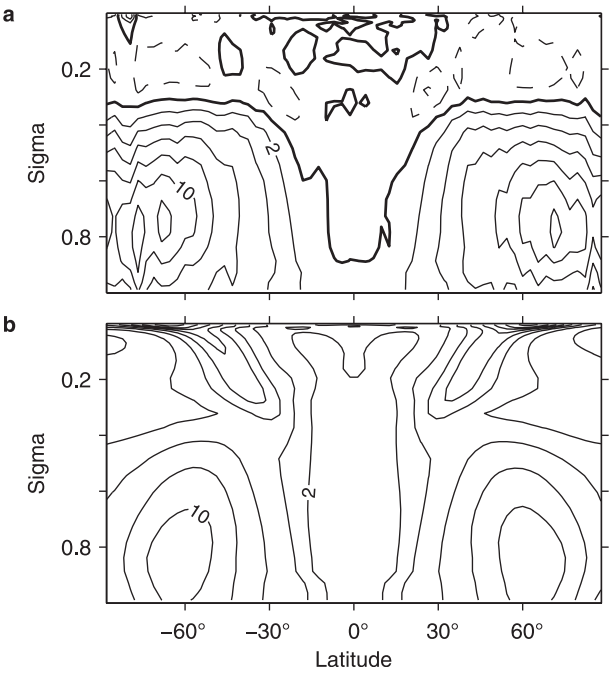


FIG. 7. (a) Temperature difference $T_e - \overline{T}$ between the temperature corresponding to the 99.9th percentile of precipitation and the mean temperature for the reference simulation. Positive values indicate that it is warmer than average when the extreme precipitation occurs. (b) $1.7T_{\text{rms}}$ corresponding to the approximation (5). Positive contours (solid line), negative contours (dashed line), and zero contour (thicker line) are shown. The contour interval is 2 K.

The precipitation extremes scaling can be expected to hold most accurately for the highest percentiles of precipitation because it does not take account of changes in the time or distance before an air parcel reaches saturation or before the onset of convection (cf. O'Gorman and Schneider 2006, 2008a). Only for the strongest updraft velocities is it reasonable to assume that saturation has already been reached or convection is occurring. The fractional rates of increase with temperature at the reference simulation of the scaling and of the precipitation extremes are compared in Fig. 5. The scaling depends on the percentile considered because it involves the temperature of extreme precipitation, although this dependence is weak, especially in the tropics or for global-mean quantities. Figure 5 suggests that the rate of change of the precipitation extremes has not yet reached an asymptotic limit at the highest percentile considered here, although the fractional rates of change of the scaling and of simulated extremes are similar for high percentiles.

The precipitation in the idealized GCM is a combination of grid-scale precipitation and convective precipitation. The precipitation extremes scaling works

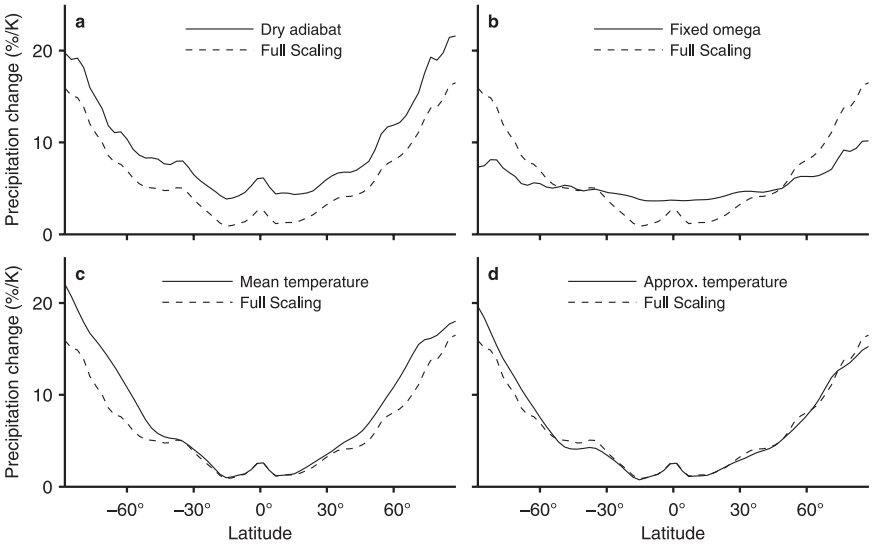


FIG. 8. Simplified variations of the precipitation extremes scaling (4) for the 99.9th percentile precipitation. Full scaling (dashed lines). (a) Not accounting for changes in the moist-adiabatic lapse rate by using the dry-adiabatic lapse rate in (2) to calculate $dq_s/dp|_{\theta^*}$, (b) holding $\omega_{\rm rms}$ fixed at its reference simulation values, (c) using mean temperature instead of the temperature of the precipitation extremes $T_e$, and (d) using the approximation $T_e = \overline{T} + 1.7T_{\rm rms}$ (solid lines). Values shown are fractional changes between the reference simulation ($\alpha = 1$) and a warmer simulation ($\alpha = 1.4$), expressed relative to the reference simulation values and normalized by the change in global-mean surface temperature (cf. with Fig. 2). The changes shown have been smoothed in latitude with a 1–2–1 filter.

roughly equally well for both types of precipitation individually (not shown). One exception is grid-scale precipitation in the tropics, the growth of which is incorrectly estimated by the scaling, but is generally only a small fraction of the total tropical precipitation. The discrepancy is likely related to changes in the fraction of tropical precipitation that is grid scale as the climate changes. As in the case of mean precipitation, extremes in convective precipitation dominate in the tropics, whereas extremes in grid-scale precipitation are larger at high latitudes.

The accuracy of the precipitation extremes scaling for the higher-resolution (T85) runs is similar to that for the T42 simulations shown in Figs. 1, 2, 4, and 5.

### c. *Importance of different components of the scaling*

The precipitation extremes scaling (4) differs from Clausius–Clapeyron scaling because of changes in the moist-adiabatic lapse rate and vertical velocity statistics, and because the temperature at which precipitation extremes occur differs from the mean temperature. The importance of each of these factors is assessed in Fig. 8 by applying simplified scalings to a difference between two simulations.

Figure 8a shows that changes in the moist-adiabatic lapse rate lower the rate of increase in precipitation extremes with warming and are influential at all latitudes. The effect is strongest in the warm low latitudes when normalized by the local rather than global change in surface temperature, consistent with the smaller fractional rate of change of the moist-adiabatic derivative of saturation specific humidity with temperature at high temperatures (Fig. 6). Inclusion of changes in the moist-adiabatic lapse rate reduces the global-mean rate of increase in the scaling from 7.3% to 4.1% $\rm K^{-1}$. The corresponding rate of increase for 99.9th percentile precipitation is 4.5% $\rm K^{-1}$, and for global-mean water vapor it is 8.9% $\rm K^{-1}$.[5]

Figure 8b shows that changes in vertical velocity statistics are also important, but with different effects at different latitudes. There are decreases with warming in $\omega_{\rm rms}$ at low latitudes but increases at high latitudes. This may be partly due to a poleward shift of the storm track with warming (Yin 2005; O'Gorman and Schneider 2008a). The decrease in $\omega_{\rm rms}$ at low latitudes is consistent with a decrease in tropical convective mass fluxes

[5] The rates of increase cited in this section are based on a two-climate estimate for a global-mean increase in surface temperature of 6.1 K, and are relative to the colder climate. Therefore, they differ from rates of increase cited elsewhere in the paper, which are based on the derivative of a spline approximation of values over the full range of climates.

found in global warming simulations (Held and Soden 2006; Vecchi et al. 2006; Vecchi and Soden 2007). In the global mean, inclusion of changes in $\omega_{\rm rms}$ reduces the rate of increase in the scaling from 4.7% to 4.1% $K^{-1}$. In a statistical analysis based on midtropospheric vertical velocity, Emori and Brown (2005) also found a negative effect of changes in vertical velocity statistics on the global-mean increase in extreme precipitation with global warming.

Figure 8c shows that using the precipitation extremes temperature $T_e$ rather than the mean temperature affects the scaling primarily in middle to high latitudes (consistent with Fig. 7a). The effect of using $T_e$ is to reduce the rate of increase in the scaling with temperature. This is partly because $T_e$ is higher than the mean temperature, and the fractional rate of increase in the moist-adiabatic derivative of saturation specific humidity is smaller at higher temperatures (Fig. 6). It is also because $T_e$ increases less quickly than the mean temperature in middle to high latitudes as the climate warms. The global-mean effect of using $T_e$ rather than the mean temperature is to reduce the fractional rate of increase in the scaling from 5.2% to 4.1% $K^{-1}$.

The precipitation extremes temperature $T_e$ makes it more difficult to use the scaling for predictions because it requires a priori knowledge of the daily precipitation amounts and temperatures. It is therefore desirable to have a simple approximation for $T_e$. Figure 7 shows that

$$T_e \simeq \overline{T} + 1.7T_{\rm rms} \tag{5}$$

is a rough estimate in the troposphere in the case of the 99.9th percentile, where $T_{\rm rms}$ is the rms eddy temperature field. Figure 8d shows that the use of this estimate successfully captures much of the effect of $T_e$ on the scaling, with a global-mean rate of change of 4.0% $K^{-1}$, which is close to the full scaling value of 4.1% $K^{-1}$. The difference $T_e - \overline{T}$ does not strongly vary with percentile for high percentiles, and the use of the approximation (5) is also adequate for the 99th and 99.99th percentiles. Further approximation of $T_{\rm rms}$ using the meridional temperature gradient could also be made to yield a mean field approximation for $T_e$.

## 5. Conclusions

We have examined the behavior of precipitation extremes in an idealized setting over a wide range of climates. Precipitation extremes generally increase at all latitudes with increasing surface temperatures, but they do not increase at the rate given by Clausius–Clapeyron scaling. In fact, extratropical precipitation extremes scale more similarly to mean precipitation than to water vapor content in our idealized GCM. In the extratropics, Pall et al. (2007) also generally found increases in extreme precipitation that were smaller than that implied by Clausius–Clapeyron scaling. However, in contrast with our results, Pall et al. (2007) found a greater increase in extreme precipitation than is given by Clausius–Clapeyron scaling in the deep tropics. Kharin et al. (2007) noted large intermodel discrepancies in the change in tropical precipitation extremes in global warming simulations. Such intermodel discrepancies in the modeling of precipitation extremes in the tropics may be related to subgrid parameterizations of deep convection.

A simple, physically based scaling captures the behavior of the precipitation extremes in the idealized GCM and shows why they need not obey Clausius–Clapeyron scaling. Changes in the moist-adiabatic lapse rate reduce the increase in precipitation extremes with global-mean surface temperature. This is most important for the scaling of precipitation extremes in the warmest regions, but it plays a significant role at all latitudes. We expect this component of the scaling to be important regardless of model specifics; it implies that tropical precipitation extremes should scale more similarly to near-surface specific humidity than to atmospheric water vapor content (section 4a).

Changes in the statistics of the vertical velocity also affect precipitation extremes. The precipitation extremes scaling uses the rms eddy vertical velocity to capture the effects of changes in vertical velocity statistics, and this appears to be adequate for the extremes in the idealized GCM. Whether such an approximation is adequate for the effects of climate change on precipitation extremes in nature is unclear. For example, the vertical velocity is not expected to have a Gaussian distribution (and does not in the idealized GCM), and updrafts are generally stronger and occupy a smaller area than downdrafts. The skewness of vertical velocity or the area of updrafts could potentially change as climate changes, and such changes may not be correctly captured in GCMs because of limited resolution. The consideration of precipitation averaged over a day and over a grid box may reduce the importance of such changes for the scaling of precipitation extremes. We find sensitivity to model spatial resolution for the magnitude of the precipitation extremes, but little sensitivity for the fractional rate of increase in precipitation extremes with climate change.

In middle to high latitudes, the temperature when precipitation extremes occur is different from the mean temperature and this reduces the increase with mean temperature of the precipitation extremes. If temperatures are higher when precipitation extremes occur because of poleward movement of air masses, then the

precipitation extremes at a given latitude may be more strongly tied to changes in mean temperature farther equatorward, rather than to the local mean temperature. Our precipitation extremes scaling involves the temperature when precipitation extremes occur, which may make the scaling less useful for prediction. However, the temperature when precipitation extremes occur can be roughly approximated using the mean temperature and the temperature variance, and so a simpler scaling of comparable accuracy may be constructed.

Our study is based on aquaplanet simulations, and so it does not directly address either orographic precipitation or the effects of land–ocean contrast, although similar considerations regarding changes in the moist-adiabatic lapse rate will apply to the scaling of orographic precipitation extremes (cf. Kirshbaum and Smith 2008). While quantitative details of changes in extreme precipitation in the idealized GCM may depend, for example, on the specific convection scheme, our results strongly suggest that no basic physical principle guarantees Clausius–Clapeyron scaling for precipitation extremes, and we have identified several factors that will cause deviations from Clausius–Clapeyron scaling.

*Acknowledgments.* We are grateful for support by the National Science Foundation (Grant ATM-0450059) and a David and Lucile Packard Fellowship. The simulations were performed on Caltech's Division of Geological and Planetary Sciences Dell cluster. Some preliminary results of this work were reported in Schneider and O'Gorman (2007).

## REFERENCES

Allen, M. R., and W. J. Ingram, 2002: Constraints on future changes in climate and the hydrologic cycle. *Nature,* **419,** 224–232.

Betts, A. K., 1998: Climate-convection feedbacks: Some further issues. *Climatic Change,* **39,** 35–38.

——, and Harshvardhan, 1987: Thermodynamic constraint on the cloud liquid water feedback in climate models. *J. Geophys. Res.,* **92,** 8483–8485.

Chen, C. T., and T. Knutson, 2008: On the verification and comparison of extreme rainfall indices from climate models. *J. Climate,* **21,** 1605–1621.

Emori, S., and S. J. Brown, 2005: Dynamic and thermodynamic changes in mean and extreme precipitation under changed climate. *Geophys. Res. Lett.,* **32,** L17706, doi:10.1029/2005GL023272.

Frierson, D. M. W., 2007: The dynamics of idealized convection schemes and their effect on the zonally averaged tropical circulation. *J. Atmos. Sci.,* **64,** 1959–1976.

Groisman, P. Y., R. W. Knight, D. R. Easterling, T. R. Karl, G. C. Hegerl, and V. N. Razuvaev, 2005: Trends in intense precipitation in the climate record. *J. Climate,* **18,** 1326–1350.

Held, I. M., and B. J. Soden, 2006: Robust responses of the hydrological cycle to global warming. *J. Climate,* **19,** 5686–5699.

Iribarne, J. V., and W. L. Godson, 1981: *Atmospheric Thermodynamics.* 2nd ed. *Geophysics and Astrophysics Monogr.,* D. Reidel, 259 pp.

Kharin, V. V., F. W. Zwiers, X. Zhang, and G. C. Hegerl, 2007: Changes in temperature and precipitation extremes in the IPCC ensemble of global coupled model simulations. *J. Climate,* **20,** 1419–1444.

Kirshbaum, D. J., and R. B. Smith, 2008: Temperature and moist-stability effects on midlatitude orographic precipitation. *Quart. J. Roy. Meteor. Soc.,* **134,** 1183–1199.

Lenderink, G., and E. van Meijgaard, 2008: Increase in hourly precipitation extremes beyond expectations from temperature changes. *Nature Geosci.,* **1,** 511–514.

Lorenz, D. J., and E. T. DeWeaver, 2007: The response of the extratropical hydrological cycle to global warming. *J. Climate,* **20,** 3470–3484.

O'Gorman, P. A., and T. Schneider, 2006: Stochastic models for the kinematics of moisture transport and condensation in homogeneous turbulent flows. *J. Atmos. Sci.,* **63,** 2992–3005.

——, and ——, 2008a: The hydrological cycle over a wide range of climates simulated with an idealized GCM. *J. Climate,* **21,** 3815–3832.

——, and ——, 2008b: Energy of midlatitude transient eddies in idealized simulations of changed climates. *J. Climate,* **21,** 5797–5806.

Pall, P., M. R. Allen, and D. A. Stone, 2007: Testing the Clausius–Clapeyron constraint on changes in extreme precipitation under $CO_2$ warming. *Climate Dyn.,* **28,** 351–363.

Schneider, T., and P. A. O'Gorman, 2007: Precipitation and its extremes in changed climates. *Extreme Events: Proc. 'Aha Huliko'a Hawaiian Winter Workshop,* Honolulu, HI, University of Hawaii at Manoa, 61–66.

——, and ——, 2008: Moist convection and the thermal stratification of the extratropical troposphere. *J. Atmos. Sci.,* **65,** 3571–3583.

Sun, Y., S. Solomon, A. Dai, and R. W. Portmann, 2007: How often will it rain? *J. Climate,* **20,** 4801–4818.

Trenberth, K. E., 1999: Conceptual framework for changes of extremes of the hydrological cycle with climate change. *Climatic Change,* **42,** 327–339.

——, A. Dai, R. M. Rasmussen, and D. B. Parsons, 2003: The changing character of precipitation. *Bull. Amer. Meteor. Soc.,* **84,** 1205–1217.

Vecchi, G. A., and B. J. Soden, 2007: Global warming and the weakening of the tropical circulation. *J. Climate,* **20,** 4316–4340.

——, ——, A. T. Wittenberg, I. M. Held, A. Leetmaa, and M. J. Harrison, 2006: Weakening of tropical Pacific atmospheric circulation due to anthropogenic forcing. *Nature,* **441,** 73–76.

Wilcox, E. M., and L. J. Donner, 2007: The frequency of extreme rain events in satellite rain-rate estimates and an atmospheric general circulation model. *J. Climate,* **20,** 53–69.

Yin, J. H., 2005: A consistent poleward shift of the storm tracks in simulations of 21st century climate. *Geophys. Res. Lett.,* **32,** L18701, doi:10.1029/2005GL023684.